A barotropic inverse tidal model for the Arctic Ocean

L. Padman[1] and S. Erofeeva[2]

Received 5 November 2003; accepted 30 December 2003; published 24 January 2004.

[1] We describe high-resolution (5-km grid) linear-dynamics and inverse models of Arctic Ocean barotropic tides obtained with the OSU Tidal Inversion Software (OTIS) package. The 8-constituent dynamics-based model uses the latest "IBCAO" bathymetry, and open boundary forcing from the recent TPXO.6.2 global barotropic tidal solution. This model performs significantly better than the present benchmark Arctic tidal model (14-km grid) by Z. Kowalik and A. Proshutinsky, as judged by comparisons with ~300 coastal tide gauges. The greatest improvements are found in the Canadian Arctic Archipelago, Nares Strait, and the Baffin Bay and Labrador Sea, and can be explained by the higher resolution of the new model in these topographically complex regions. The new Arctic inverse model assimilates coastal and benthic tide gauges and TOPEX/Poseidon and ERS altimetry for further improvements of the 4 dominant constituents M_2, S_2, K_1 and O_1. *INDEX TERMS:* 4207 Oceanography: General: Arctic and Antarctic oceanography; 4560 Oceanography: Physical: Surface waves and tides (1255); 4556 Oceanography: Physical: Sea level variations. **Citation:** Padman, L., and S. Erofeeva (2004), A barotropic inverse tidal model for the Arctic Ocean, *Geophys. Res. Lett.*, *31*, L02303, doi:10.1029/2003GL019003.

1. Introduction

[2] Tides contribute significantly to general patterns of hydrography and circulation in the world ocean through their effect on mixing in the ocean interior [e.g., *Munk and Wunsch*, 1998]. This also holds true in high-latitude seas [e.g., *Padman*, 1995]. Tidal currents also help set the characteristics of the sea-ice cover including open-water ("lead") fraction [*Kowalik and Proshutinsky*, 1994 (hereinafter denoted KP-94); *Padman and Kottmeier*, 2000], and thus modify the efficiency of the sea ice as a barrier to heat and fresh water exchanges between the ocean and atmosphere.

[3] Tide heights in deep water are now well constrained by TOPEX/Poseidon ("T/P") satellite altimetry equatorward of the satellite's turning latitude of ~66° [*Shum et al.*, 1997]. Polar regions are, however, only poorly sampled by satellite altimetry: the ERS satellites have a turning latitude of ~82°, but cannot provide high-quality data when sea ice is present and have poor orbital characteristics for resolving some major tidal harmonics. We have previously reported improved tide models for the Antarctic [*Padman et al.*, 2002, 2003]. Here, we document a new, high-resolution model of Arctic Ocean barotropic tides using assimilation of tide height data. The study's short-term goal is to create an accurate model of Arctic barotropic tides. In the longer-term, the model will be used as a benchmark for quantifying improvements to dynamics-based Arctic tide models through increased resolution and improved physical representation of tidal energy dissipation processes.

2. The New Tide Models

2.1. Model Domain

[4] The model domain (Figure 1) is based on the International Bathymetric Chart of the Arctic Ocean ("IBCAO") [*Jakobsson et al.*, 2000] digitized onto a uniform 5-km grid. The domain includes all of the central Arctic Ocean, the Greenland Sea, the Labrador Sea and Baffin Bay, and the Canadian Arctic Archipelago ("CAA"). There are two features of this domain that will be relevant to further discussions. First, a significant fraction of the Arctic Ocean's area is covered by the broad continental shelf seas of the eastern (or Eurasian) Arctic. Second, the passages of the CAA are narrow, and the flow of tidal energy through the CAA critically depends on adequate resolution of these passages. As with other tide modeling efforts, the quality of dynamics-based models also depends to a large extent on the accuracy of the bathymetry grid.

2.2. Tide Height Data

[5] We have identified 310 coastal and benthic tide gauge records in the model domain that provide tidal coefficients for at least a few of the most energetic tidal harmonics [KP-94; *Tidal Tables*, 1941, 1958]; for locations, see Figure 1. Data are also available from the T/P and ERS-1 and ERS-2 satellite radar altimeters: T/P measures sea surface height (SSH) for ice-free ocean to ~66°N, while the ERS satellites measure SSH for ice-free ocean to ~82°N. The T/P orbit was designed to allow tides to be accurately measured [*Parke et al.*, 1987]. Individual ERS height measurements are of lower accuracy than T/P, the orbit is unfavorable for resolving solar constituents (e.g., S_2 and K_1), and the higher-latitude data must frequently be discarded because of sea ice within the radar's footprint. Nevertheless, for some constituents the ERS data set provides useful information about ocean tides north of the T/P ground track.

[6] The tide gauge ("TG") data set has been divided into 7 regions (see Figure 1) to simplify comparisons between various tide models and data. This division is based primarily on geographic features, but also considers the spatial variations in the amplitudes of semidiurnal and diurnal tides.

2.3. The Dynamics-Based Model

[7] The first step towards an inverse tidal solution is development of a dynamics-based "prior" model. The Arctic Ocean Dynamics-based Tide Model (AODTM) is the numerical solution to the shallow water equations (SWE), which are essentially linear. We solve the SWE

[1]Earth & Space Research, Corvallis, Oregon, USA.
[2]College of Oceanic & Atmospheric Sciences, Oregon State University, Corvallis, Oregon, USA.

Copyright 2004 by the American Geophysical Union.
0094-8276/04/2003GL019003$05.00

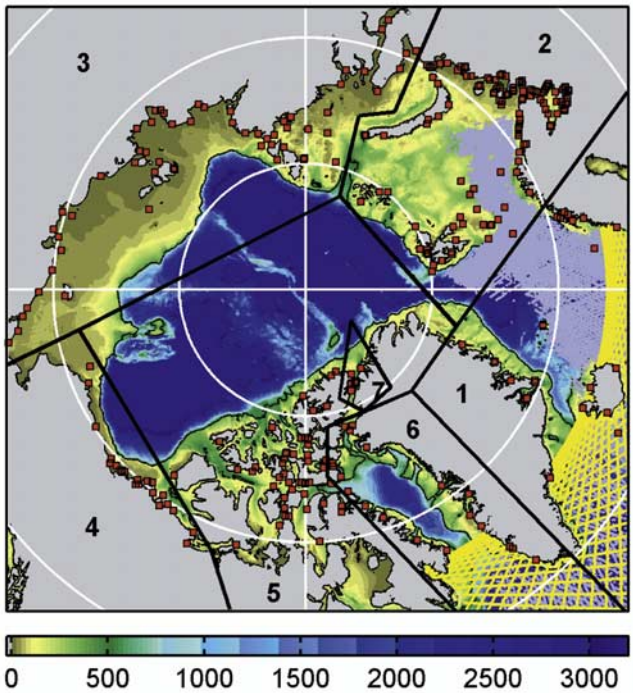

Figure 1. Model domain, showing locations of tide gauge data (red squares), and ERS and TOPEX/Poseidon radar altimetry (lilac and yellow dots, respectively). The color scale is water depth (m); the 500 m isobath is shown as a black line. The domain is partitioned into 7 regions for model-data comparisons (see Table 1). These regions are: (1) North Atlantic; (2) Barents Sea (including the White Sea); (3) the Russian shelf seas (Kara, Laptev, East Siberian, Chukchi); (4) the northern coast of Alaska and the Canadian Northwest Territories; (5) the Canadian Arctic Archipelago; (6) Baffin Bay and the Labrador Sea; and (7) Nares Strait at the northern end of Baffin Bay.

by direct matrix factorization for 8 harmonics: M_2, S_2, N_2, K_2, K_1, O_1, P_1, and Q_1; see *Egbert and Erofeeva* [2002] (hereinafter denoted E&E). Potentially significant simplifications to the SWE dynamics include our use of: tidal loading and self attraction computed from a 1/4° global tidal solution TPXO6.2; and the use of linear benthic friction, $\mathbf{F} = (r/H)\mathbf{U}$, where r is the friction velocity, H is the water depth, and $\mathbf{U}$ is the depth-integrated transport (see E&E for more details). The TPXO6.2 model (http://www.oce.orst.edu/po/research/tide/global.html) is an updated version of TPXO3 [*Egbert*, 1997]. We use $r = 0.5$ m s^{-1} for semi-diurnal constituents and $r = 2$ m s^{-1} for diurnals. The larger value for diurnal constituents is required because diurnal currents are frequently strongest in relatively deep water along the shelf break. We assume that the errors introduced by the simplified dynamics can be corrected by the data assimilation. The AODTM uses elevations taken from TPXO6.2 as open ocean boundary conditions. Additional forcing is provided by the specified astronomical tide potentials.

2.4. The Inverse Model

[8] The Arctic Ocean Tidal Inverse Model (AOTIM) was created following the data assimilation scheme described by *Egbert et al.* [1994] (hereinafter denoted EBF), *Egbert* [1997], and E&E. Only the 4 most energetic tides (M_2, S_2, O_1, and K_1) were simulated with AOTIM: for prediction purposes we use N_2, K_2, P_1, and Q_1 from AODTM. Assimilated data consists of coastal and benthic tide gauges (between 250 and 310 gauges per constituent), 364 cycles of T/P and 108 cycles of ERS altimeter data from a modified version of the "Pathfinder" database [*Koblinsky et al.*, 1999] with no tidal corrections applied [B. Beckeley, personal communication, 2003]. We used T/P altimeter data for 11178 data sites with a spacing of ~7 km, and ERS altimeter data for 18224 data sites, shown in Figure 1. For M_2 and O_1 we assimilated TG, T/P and ERS data. For K_1 we used TG and T/P data, and for S_2 we used TG data only. These choices are based on the ability of the satellite data to resolve specific harmonics depending on orbit characteristics; see, e.g., *Smith et al.* [2000].

[9] The dynamical error covariance was defined following EBF, using the AODTM as a "prior" solution to estimate the spatially varying magnitudes of errors in the momentum equations. The correlation length scale for the dynamical errors was set to 50 km (10 grid cells). The continuity equation was assumed to be exact.

[10] To compute the inverse solution we used the single-constituent reduced basis approach [EBF] to calculate the representer coefficients. The efficient calculation scheme described by E&E was applied. The most significant changes from the prior solution for the semidiurnals were in the Barents Sea near the entrance into the White Sea (amplitude changes >60 cm for M_2 and >30 cm for S_2), in

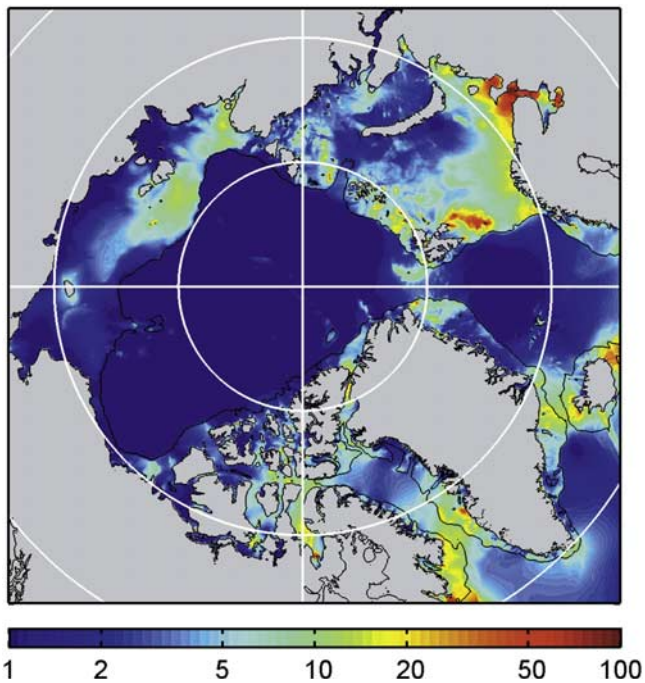

Figure 2. Mean tidal current speed (cm s^{-1}) based on simulating 14 days of hourly total tidal speed from the 8-constituent inverse solution AOTIM. A logarithmic color scale is used to resolve speed variability in both weak and energetic regions. The black contour shows the 500 m isobath. The largest values approach 100 cm s^{-1} in the southern Barents Sea near the entrance to the White Sea and around Bear Island in the western Barents Sea south of Svalbard.

Table 1. Signal Strength (Root-Mean-Square Tide Height Amplitude), and Root-Mean-Square Tide Height Misfits (RMS_{RI}, See equation (1)) between 4 Arctic Models and Sets of Tide Gauge Data, for the 4 Most Energetic Tidal Harmonics, M_2, S_2, K_1 and O_1

M_2	Signal	KP-94	AODTM	TPXO6.2	AOTIM
All	72	25.4	18.3	19.6	8.4
1	69	14.5	15.9	11.4	9.6
2	94	34.8	25.3	28.0	10.0
3	16	9.1	8.6	6.8	4.7
4	16	9.0	9.2	10.9	8.8
5	44	20.3	6.0	5.6	3.9
6	87	17.7	14.5	13.2	11.8
7	52	9.2	4.2	4.6	3.5
S_2	Signal	KP-94	AODTM	TPXO6.2	AODTM
All	22	9.4	7.6	6.8	2.1
1	25	7.5	5.7	7.8	2.3
2	25	11.6	10.5	8.9	2.4
3	8	4.4	4.4	3.9	1.6
4	5	3.4	2.9	4.1	1.1
5	17	7.1	2.6	3.2	1.8
6	37	14.8	6.5	5.0	2.5
7	21	9.7	2.2	3.2	1.9
K_1	Signal	KP-94	AODTM	TPXO6.2	AOTIM
All	6	6.3	6.1	3.9	2.4
1	2	2.1	2.2	2.3	2.3
2	5	4.9	7.4	3.7	2.8
3	3	3.4	2.3	2.2	1.7
4	3	2.5	1.3	3.3	1.1
5	9	9.5	6.5	6.0	2.1
6	14	13.7	7.6	3.6	2.9
7	5	4.5	1.6	3.2	1.1
O_1	Signal	KP-94	AODTM	TPXO6.2	AOTIM
All	5	3.0	1.9	1.8	1.4
1	6	1.5	1.2	1.0	1.1
2	3	2.2	2.0	1.8	1.4
3	3	1.6	1.5	1.2	1.5
4	3	8.2	1.0	1.4	0.9
5	9	4.2	2.3	2.6	1.4
6	11	6.7	2.6	1.7	1.7
7	4	1.6	0.7	1.7	0.3

All values have units of cm. The 4 models are; the dynamics-only models by *Kowalik and Proshutinsky* [1994] (KP-94) and the Arctic Ocean Dynamics-based Tide Model (AODTM: this paper), and the inverse models TPXO6.2 (global solution) and the Arctic Ocean Tidal Inverse Model (AOTIM: this paper). Results are presented for the entire domain ("All"), and for the 7 subdomains shown in Figure 1.

All - Subset of KP-94 tide gauge data base plus additional sites in the Barents/White Seas, number of sites: 310(M_2), 275(S_2), 276(K_1), 250(O_1). 1-North Atlantic, number of sites: 23(M_2), 20(S_2), 19(K_1), 16(O_1). 2-Barents and White Seas, number of sites: 134(M_2), 117(S_2), 127(K_1), 103(O_1). 3-Russian Seas, number of sites: 57(M_2), 52(S_2), 44(K_1), 44(O_1). 4-Alaskan Coast, number of sites: 22(M_2), 19(S_2), 17(K_1), 17(O_1). 5-Canadian Arctic Archipelago, number of sites: 46(M_2), 46(S_2), 46(K_1), 46(O_1). 6-Baffin Bay and Labrador Sea, number of sites: 19(M_2), 14(S_2), 16(K_1), 17(O_1). 7-Nares Strait, number of sites: 7(M_2), 6(S_2), 7(K_1), 7(O_1).

the White Sea (>40 cm for M_2 and >10 cm for S_2) and in the northern part of Baffin Bay (>20 cm for M_2 and >10 cm for S_2). The most significant changes from the prior solution for the diurnals were in the Baffin Bay and the Gulf of Boothia in the CAA (maximum amplitude changes ~20 cm for K_1 and ~5 cm for O_1), in the Barents Sea near the entrance to the White Sea (~10 cm for both K_1 and O_1), and in the Greenland Sea (~10 cm for K_1 and ~5 cm for O_1).

3. Results

[11] Maps of tide height amplitude and phase are qualitatively similar to previously published maps (e.g., Figures 2–5 in KP-94) and so are not shown here. Averaged over the entire model domain, the M_2, S_2, K_1 and O_1 tides account for 79%, 10%, 5% and 1% of the total (8-constituent) tidal potential energy, respectively. That is, Arctic tide height variability is overwhelmingly dominated by M_2, whose amplitude exceeds 1 m in the southern Barents Sea near the entrance to the White Sea, in the Labrador Sea, and at the northern end of Baffin Bay. The distribution of S_2 amplitude is similar to M_2, but is about a factor of 3 smaller. Diurnal tide amplitudes are largest in Baffin Bay and the Labrador Sea ("BBLS") and in the Gulf of Boothia in the southern CAA. Maximum amplitudes are ~0.4 m for K_1, and about 0.2 m for O_1.

[12] We calculate root-mean-square (RMS) errors averaged over the in-phase and quadrature components for each constituent, i.e.,

$$RMS_{RI} = \left(\frac{1}{2N}\sum_{i=1}^{N}\left(\left[\mathrm{Re}\left(\hat{z}^l(\mathbf{x}_i) - z_0^l(\mathbf{x}_i)\right)\right]^2 + \left[\mathrm{Im}\left(\hat{z}^l(\mathbf{x}_i) - z_0^l(\mathbf{x}_i)\right)\right]^2\right)\right)^{1/2}, \quad (1)$$

where $\hat{z}^l$ $(\mathbf{x}_i)$ and $z_0^l(\mathbf{x}_i)$ are the measured and modeled harmonic constants, respectively, for constituent l at location $\mathbf{x}_i$, and the sum is over N data sites. For conciseness, we present averaged error values for the 7 subdomains described in section 2.2 (see Figure 1). Table 1 lists the value of RMS_{RI} for the comparison of TG data with 4 models; KP-94, AODTM, TPXO6.2, and AOTIM. Since both TPXO6.2 and AOTIM have assimilated these data, the fits in these cases represent the assigned uncertainty in data coefficients and the effect of other assumptions in the inverse calculation.

[13] Averaged over the entire domain, the new dynamics-based model AODTM performs significantly better than KP-94 for the dominant M_2 tide, with smaller but significant improvements for S_2 and O_1. The improvement from KP-94 to AODTM is most pronounced for all 4 constituents in the topographically complex region of the CAA, BBLS and Nares Strait (regions 5–7 in Figure 1): we attribute this result primarily to the higher resolution of AODTM, 5 km vs. 14 km for KP-94. The K_1 diurnal constituent in AODTM is less accurate than in KP-94 for the Barents and White Seas: as yet we have no explanation for this result. Our studies indicate that dynamics-based models of diurnal tides are sensitive to the location of the open boundary south of Davis Strait: we chose the location that minimizes RMS_{RI} in AODTM for the BBLS region.

[14] As required by the assimilation approach, the errors for the 2 inverse models, TPXO6.2 and AOTIM, are smaller than for either dynamics-based model. For semidiurnal tides, AOTIM is a significantly better fit to the tide gauge data than is TPXO6.2. This improvement is explained by the higher resolution of AOTIM (5 km vs. 1/4° for TPXO6.2), and because the decorrelation length scale for TPXO6.2 is 250 km, which does not allow as accurate a fit to closely spaced tidal data in complex regions as can be achieved with the 50 km scale used in AOTIM. The closer correspondence between the errors for the 2 inverse models for diurnal tides arises because the accuracy

of each solution is approaching the assumed data error in most subregions.

4. Discussion and Conclusions

[15] While the new models have been validated against tide height data (see Table 1), most oceanographic interest in tides is related to the strength and gradients of tidal currents rather than height variations. We assume that the high-resolution data assimilation model AOTIM, which best fits the available tide height data, also best represents tidal currents. This is a reasonable assumption since the inverse model is consistent with the shallow-water wave equations to within the assumed accuracy of the bathymetry-based and dissipation terms. For each grid node **x** in the model domain we calculate the time-averaged magnitude of tidal velocity:

$$\bar{u}(\mathbf{x}) = \frac{1}{T}\sum_{i=1}^{T}\left(\left(\sum_{k=1}^{8} u_k(\mathbf{x}, t_i)\right)^2 + \left(\sum_{k=1}^{8} v_k(\mathbf{x}, t_i)\right)^2\right)^{1/2}. \quad (2)$$

In (2), u_k and v_k are east and north components of velocity for the k'th tidal harmonic, and the summation $k = 1, 2, \ldots, 8$ is of the 8 modeled harmonics at location **x** and time t_i. The mean speed is the average of $T = 336$ hourly modeled tidal current speeds over a time interval of 14 days, which encompasses the beat periods of the 4 major constituents. The calculation includes the slow periodic time variations associated with the "nodal" (~18.6 y period) tide modulation; see E&E for further details.

[16] The map of $\overline{u}$ (Figure 2) is qualitatively similar to the map of "maximum tidal current" $u_{\max}$ plotted by KP-94 (their Plate 1): in general, $u_{\max} \approx 2\,\overline{u}$. The largest currents are over the broad Eurasian shelf seas, with typical values for $\overline{u}$ of ~5–15 cm s^{-1}. Values of $\overline{u} > 50$ cm s^{-1} are found in the western Barents Sea south of Bear Island [see *Kowalik and Proshutinsky*, 1995] and in the southern Barents Sea near the entrance to the White Sea. Strong ($\overline{u} > 20$ cm s^{-1}) currents are also found in Davis Strait in the Labrador Sea, and in Nares Strait and various locations within the CAA. Currents are weak over the deep basins and along the northern coast of Alaska.

[17] We have ignored the possible effects of sea-ice cover in the present models. KP-94 note that sea ice may change tidal amplitudes by up to 10% and phases by 1–2 h, presumably leading to quasi-seasonal variability in tidal coefficients.

[18] As demanded by the assimilation approach, AOTIM is the Arctic tide model that is most consistent with available tide gauge data and satellite altimetry (not shown). Nevertheless, the long-term goal should be to develop dynamics-only models with comparable accuracy, since regions for which no tidal records are available (notably the central deep Arctic basins) will be better modeled by accurate dynamics than by extrapolation of a solution constrained by near-coastal height data. Significant improvements are likely through further increasing model resolution, adding ice-ocean interactions, and increasing the sophistication of dissipation parameterizations including benthic friction and the conversion of barotropic tidal energy to internal tides [cf., *Jayne and St. Laurent*, 2001].

[19] The model is available from http://www.oce.orst.edu/po/research/tide/Arc.html (with Fortran-based access code) and http://www.esr.org/arctic_tides_index.html (with Matlab access code).

[20] **Acknowledgments.** This work was funded by the National Science Foundation grant OPP-0125252 (LP) and NASA JASON-1 grant NCC5-711 (SE). We appreciate the assistance of A. Proshutinsky and G. Kivman in developing the data base of Arctic tide gauge harmonic constants used in this paper. The thorough and constructive comments from two anonymous reviewers are greatly appreciated, as are the efforts of Editor C. Reason.

References

Egbert, G. D. (1997), Tidal data inversion: Interpolation and inference, *Prog. Oceanogr.*, *40*, 53–80.
Egbert, G. D., A. F. Bennett, and M. G. G. Foreman (1994), TOPEX/POSEIDON tides estimated using a global inverse model, *J. Geophys. Res.*, *99*(C12), 24,821–24,852.
Egbert, G. D., and S. Y. Erofeeva (2002), Efficient inverse modeling of barotropic ocean tides, *J. Atmos. Ocean. Tech.*, *19*(2), 183–204.
Jakobsson, M., N. Cherkis, J. Woodward, B. Coakley, and R. Macnab (2000), A new grid of Arctic bathymetry: A significant resource for scientists and mapmakers, *Eos Transactions*, AGU, *81*(9), pp. 89, 93, 96.
Jayne, S. R., and L. C. St. Laurent (2001), Parameterizing tidal dissipation over rough topography, *Geophys. Res. Lett.*, *28*(5), 811–814.
Koblinsky, C. J., R. D. Ray, B. D. Beckeley, Y.-M. Wang, L. Tsaoussi, A. Brenner, and R. Williamson (1999), NASA ocean altimeter Pathfinder project report 1: Data processing handbook, NASA/TM-1998-208605.
Kowalik, Z., and A. Y. Proshutinsky (1994), The Arctic Ocean Tides, in *The Polar Oceans and Their Role in Shaping the Global Environment*, *Geophysical Monograph*, 85, edited by O. M. Johannessen, R. D. Muench, and J. E. Overland, AGU, Washington, D. C., pp. 137–158.
Kowalik, Z., and A. Y. Proshutinsky (1995), Topographic enhancement of tidal motion in the western Barents Sea, *J. Geophys. Res.*, *100*(C2), 2613–2637.
Munk, W., and C. Wunsch (1998), Abyssal recipes II: Energetics of tidal and wind mixing, *Deep Sea Res.*, *45*, 1977–2010.
Padman, L. (1995), Small-scale physical processes in the Arctic Ocean, In *Arctic Oceanography: Marginal Ice Zones and Continental Shelves*, *Coastal and Estuarine Studies*, 49, edited by W. O. Smith and J. M. Grebmeier, pp. 97–129, AGU, Washington, D. C.
Padman, L., S. Erofeeva, and I. Joughin (2003), Tides of the Ross Sea and Ross Ice Shelf cavity, *Antarc. Sci.*, *15*(01), 31–40.
Padman, L., H. A. Fricker, R. Coleman, S. Howard, and S. Erofeeva (2002), A new tidal model for the Antarctic ice shelves and seas, *Ann. Glaciol.*, *34*, 247–254.
Padman, L., and C. Kottmeier (2000), High-frequency ice motion and divergence in the Weddell Sea, *J. Geophys. Res.*, *105*(C2), 3379–3400.
Parke, M. E., R. H. Stewart, D. L. Farless, and D. E. Cartwright (1987), On the choice of orbits for an altimetric satellite to study ocean circulation and tides, *J. Geophys. Res.*, *92*, 11,693–11,707.
Shum, C. K., et al. (1997), Accuracy assessment of recent ocean tide models, *J. Geophys. Res.*, *102*(C11), 25,173–25,194.
Smith, A. J. E., B. A. C. Ambrosius, and K. F. Wakker (2000), Ocean tides from T/P, ERS-1, and GEOSAT altimetry, *J. Geodesy*, *74*, 399–413.
Tide Tables (1941), Gidrographic Board of VMF of USSR, Tidal tables (in Russian), vol. 2, Harmonic constants for tide prediction, Leningrad.
Tidal Tables (1958), Vol. 1 Waters of European part of the USSR, part 2: Tidal harmonic constants, (in Russian), Leningrad, Gidrometizdat.

L. Padman, Earth & Space Research, 3350 SW Cascade Ave., Corvallis, OR 97333-1536, USA. (padman@esr.org)
S. Erofeeva, College of Oceanic & Atmospheric Sciences, Ocean Admin Bldg 104, Oregon State University, Corvallis, OR 97331, USA.